

Article

Granular Flow Impact on Shed Tunnels and the Buffering Effect of Cushion Layers

Li Wei, Jianghong Wang and Zili Dai * 

Department of Civil Engineering, Shanghai University, 99 Shangda Road, Shanghai 200444, China; weili0319@shu.edu.cn (L.W.); wangjianghong@shu.edu.cn (J.W.)

* Correspondence: zilidai@shu.edu.cn; Tel.: +86-188-1787-9593

Abstract: Granular flow is one of the most destructive geological hazards in mountainous areas, posing a severe threat to the economy and personnel safety in the region. Shed tunnels are widely used for the prevention and mitigation of granular flow hazards. Thus, comprehensively studying the impact mechanisms of granular flows on shed tunnels is significant for disaster prevention and mitigation. This study adopts a combined approach of a physical model experiment and Particle Flow Code (PFC) simulation to investigate the impact force of granular flow on shed tunnels and the buffering effect of cushion layers. The influences of slope angle, cushion layer thickness, and cushion layer particle size are discussed. It is revealed that as the slope angle increases, the velocity of the granular flow and the impact force on the shed rise significantly. When the slope angle increases from 40° to 60°, the peak velocity surges by 25%, while the impact force intensifies by 2–3 times. Moreover, increasing the thickness of the cushion layer can mitigate the interaction between the granular flow and the shed tunnel, thereby enhancing structural safety. With an increase in cushion layer thickness from 0 to 200 mm, the impact force is reduced by approximately 50%. Meanwhile, reducing the particle size of the cushion layer effectively decreases the impact force, resulting in less kinetic energy and providing a stronger cushioning effect.

Keywords: granular flow; shed tunnel; impact force; cushion layer; PFC



Citation: Wei, L.; Wang, J.; Dai, Z. Granular Flow Impact on Shed Tunnels and the Buffering Effect of Cushion Layers. *Appl. Sci.* **2024**, *14*, 3409. <https://doi.org/10.3390/app14083409>

Academic Editor: Giuseppe Lacidogna

Received: 29 February 2024

Revised: 22 March 2024

Accepted: 13 April 2024

Published: 17 April 2024



Copyright: © 2024 by the authors. Licensee MDPI, Basel, Switzerland. This article is an open access article distributed under the terms and conditions of the Creative Commons Attribution (CC BY) license (<https://creativecommons.org/licenses/by/4.0/>).

1. Introduction

Granular flow disasters, such as mudslides, landslides, and rock avalanches, frequently occur all over the world with characteristics of large scale, high mobility, long runout distances, and significant destructive power [1–3]. They can be triggered by earthquakes, extreme climate, and various human factors and result in significant casualties and economic losses [4,5]. For example, in April 1903, a massive landslide with a volume of approximately $30 \times 10^6 \text{ m}^3$ occurred on Turtle Mountain in southwestern Alberta, Canada. The landslide traveled more than 3000 m, blocked a river, and devastated the town of Frank, resulting in the deaths of over 10,000 people [6–8]. In October 1963, a rockslide with a volume of 200–300 million m^3 occurred near the Vajont dam in Italy with a speed of 20–30 m/s, leading to 2500 deaths [9,10]. In April 1974, an enormous catastrophic rockslide with an estimated volume of 10^9 m^3 occurred in the Peruvian Andes of Peru. The rockslide traveled a vertical distance of 1.9 km at an average velocity of about 130 km/h, causing about 451 deaths and severe destruction [11]. In April 2000, a catastrophic landslide damming event occurred on the Yigong River in Tibet, China. The landslide traveled 10 km within 10 min, with a vertical drop of over 3300 m. The volume of the landslide was estimated to be $28 \times 10^7 \sim 30 \times 10^7 \text{ m}^3$, resulting in the formation of a massive landslide dam. This led to a rapid rise in water levels upstream, causing widespread flooding in surrounding villages and posing a significant threat to the lives and properties of downstream residents [12–14]. In 2008, the Wenchuan earthquake in China triggered thousands of landslide disasters. These earthquake-induced landslides were highly destructive and

resulted in approximately 20,000 deaths and significant economic losses [15–17]. Granular flow and landslide disasters are sometimes caused by their inherent factors, including topography, slope gradient, rock mechanics characteristics, and internal joints [18].

To protect mountainous roads from granular flow disasters, shed tunnels are often installed in sections prone to geological hazards. Shed tunnels serve as protective measures and effectively safeguard the road, vehicles, and pedestrians in the event of a granular flow disaster. Traditional shed tunnels can be classified into different types based on their shape and function, such as portal sheds, rectangular sheds, arched sheds, and semi-arched sheds. Usually, a cushion layer is laid on the mountain side of the shed tunnel as a suitable and effective measure of disaster mitigation. The cushion layer often consists of gravel, sand, or other buffering materials. It can absorb a portion of the impact energy from the granular flow, thereby protecting the shed structure [19,20]. However, when subjected to intense granular flow impact, the shed tunnel may still sustain damage due to excessive forces. Therefore, investigation into mitigation measures to reduce the impact force of granular flows on shed tunnels is of practical significance. Extensive research has been conducted on the dynamic impact of rolling and falling rocks on shed tunnels, as well as the dynamic response of shed tunnels [21–25]. Compared to the impact of rolling and falling rocks, granular flows have more complex mechanical properties, and they can cause damage to shed tunnels even without reaching the ultimate bearing capacity. The dynamic effects of granular flow impact on shed tunnels and the cushioning effects of the cushion layer have been investigated through methods such as model experiments, numerical simulations, and theoretical analysis [26–31]. Indeed, although there have been significant advancements in research on the dynamic impact of granular flow, there are still many unresolved challenges regarding the underlying mechanical mechanisms. Further in-depth studies are needed to fully understand the complex dynamics and destructive effects of granular flow.

This study aims to investigate the impact force of granular flow on shed tunnels and the buffering effects of the cushion layer by combining model experiments with Particle Flow Code (PFC) simulations. In this study, slope angle, cushion layer thickness, and cushion layer particle size are considered variables. The impact forces under different conditions are analyzed to investigate the impact mechanism of granular flow and the buffering effects of the gravel cushion layer. The simulation results are compared with the model experiment data, showing a high degree of similarity. This indicates that the PFC model can accurately simulate the dynamic characteristics of granular flow.

2. Methodology

2.1. Experimental Setup

The model experiment setup consists of three main parts: the source area, the transfer area, and the shed tunnel. The slope angle α can be adjusted between 40° and 60° . The dimensions of the source area are 0.4 m in length, 0.3 m in width, and 0.4 m in height. The transfer area is 2.0 m long, 0.3 m wide, and 0.4 m high. A cushion layer can be set between the slope toe and the shed tunnel, as well as on the top of the shed tunnel. The dimensions of the shed tunnel are 0.3 m in length, 0.3 m in width, and 0.15 m in height, as shown in Figure 1. The granular flow particles used in this study have a size range of 10 mm to 20 mm, and the total mass of the granular flow is 50 kg. To measure the impact forces of granular flow on each face of the shed tunnel, the individual faces of the shed tunnel are separated. Bolts are used to connect each face to sensors, and they are fixed at the slope toe. In Figure 1, F1 represents the normal impact force on the front face of the shed structure, which is measured by the force sensors S1 and S2. F2 represents the normal impact force on the top surface of the shed structure, measured by the force sensors S3 and S4.

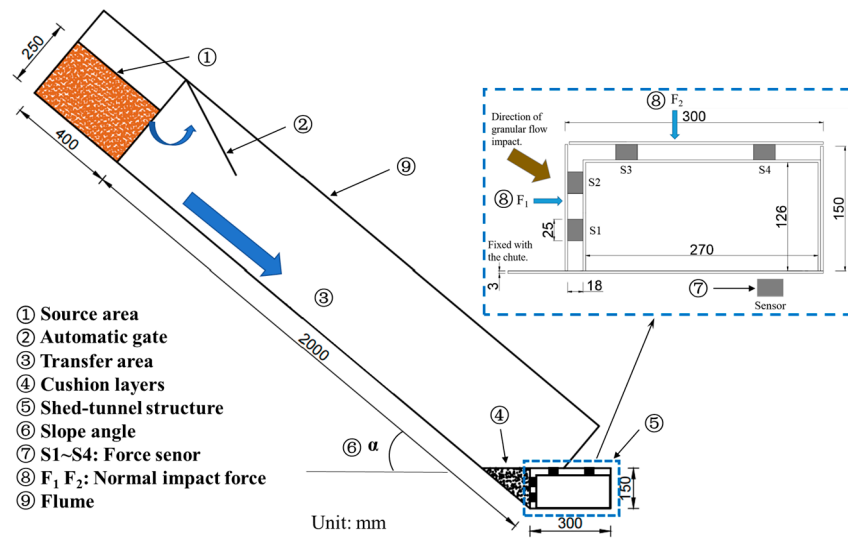


Figure 1. Model testing device and shed tunnel.

2.2. Numerical Method

The numerical simulation in this study utilizes the PFC3D 5.0 software developed by the Itasca company (Minneapolis, MN, USA), which is widely used in various fields. This software is based on the discrete element theory and simulates the behavior of macroscopic materials through the interactions among numerous discrete particles. This approach represents different materials as collections of particles with their own unique physical properties to study their mechanical performance and deformation characteristics, which depend on the structure and contact properties of individual particles. In the PFC calculation process, the motion of particles follows Newton’s second law and the force-displacement law. Particle displacements alter the contact forces between particles, which are calculated using Newton’s second law, and then the force-displacement law is applied to determine the particle displacements. This process is repeated at each time step until the unbalanced forces between particles decrease below a predefined threshold value.

To consider the influence of the moment between particles, we have chosen the linear parallel bond model in this study. This model reflects the contact between particles and between particles and walls, as shown in Figure 2. The linear parallel bond model is an extension of the linear model that incorporates parallel bonds capable of bearing bending moments. This addition allows for the transmission of both moment and bonded force when combined with the linear model. If the load exceeds the strength limit, the parallel bond will break.

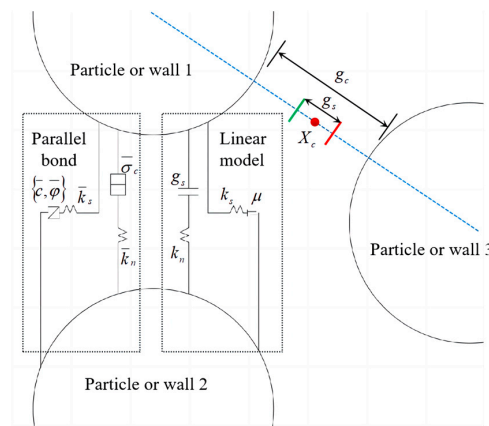


Figure 2. Schematic of the linear parallel bond model.

The numerical simulation model is established on a 1:1 scale based on the model experiment setup, as shown in Figure 3. In the PFC model, the source area is composed of 31,842 spherical particles with a density of 2650 kg/m^3 . The size of the particles is controlled at 10–20 mm, which is inconsistent with the granular material used in the model experiments. The three-dimensional geometric chute model and shed tunnel structure are constructed using wall elements, consisting of a total of 18 facets. The contacts between particles are simulated using a linear parallel bond model.

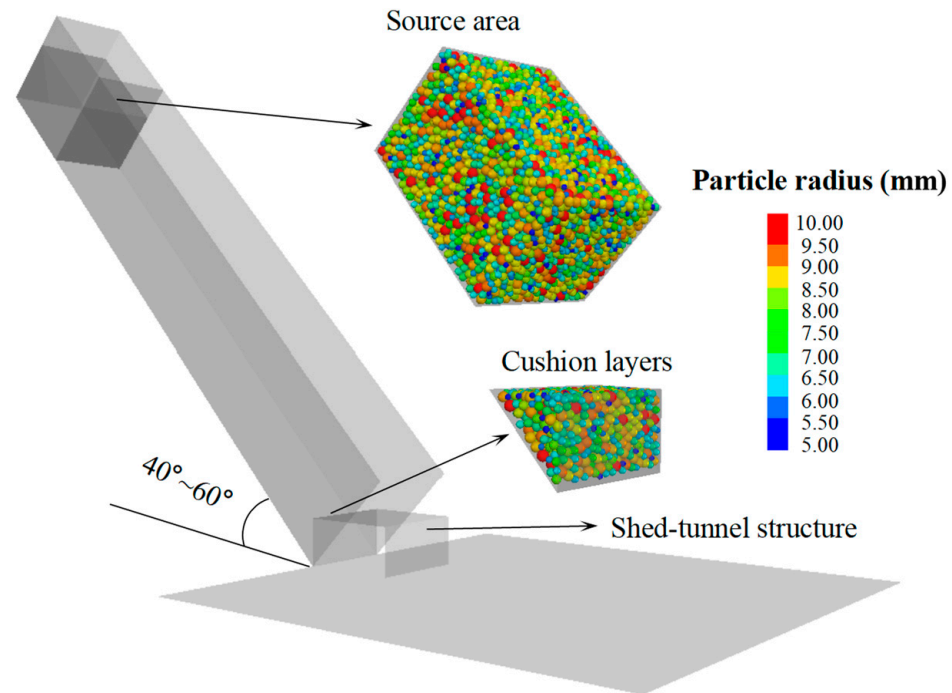


Figure 3. Model of numerical simulation.

2.3. Parameter Calibration

Due to the significant influence of microscopic parameters on the simulation results of PFC, it is important to calibrate the parameters used to ensure the accuracy of the numerical simulation results. In this study, parameter calibration is conducted through particle column collapse tests and granular flow impact tests.

In the test, a cylindrical PVC transparent pipe with dimensions of 400 mm in length and 120 mm in radius is used. The pipe is filled with 300 mm of gravel soil, and then it is lifted upward at a speed of 20 mm/s, allowing the gravel to naturally collapse onto a horizontal acrylic plate. The accumulation characteristics of the granular materials are nearly between numerical simulation and model test, as shown in Figure 4. The parameters used in the simulation are shown in Table 1.

Table 1. Parameters utilized in the numerical simulation.

Parameters	Values
Density, ρ (kg/m^3)	2650
Bond effective modulus of ball–ball, E (Pa)	2.4×10^6
Bond effective modulus of ball–facet, E' (Pa)	1.0×10^5
Bond normal-to-shear stiffness ratio, k_n/k_s (/)	1.00
Particle friction coefficient, μ_p (/)	0.50
Wall friction coefficient, μ_w (/)	0.38
Particle diameter, d (mm)	10.0–20.0

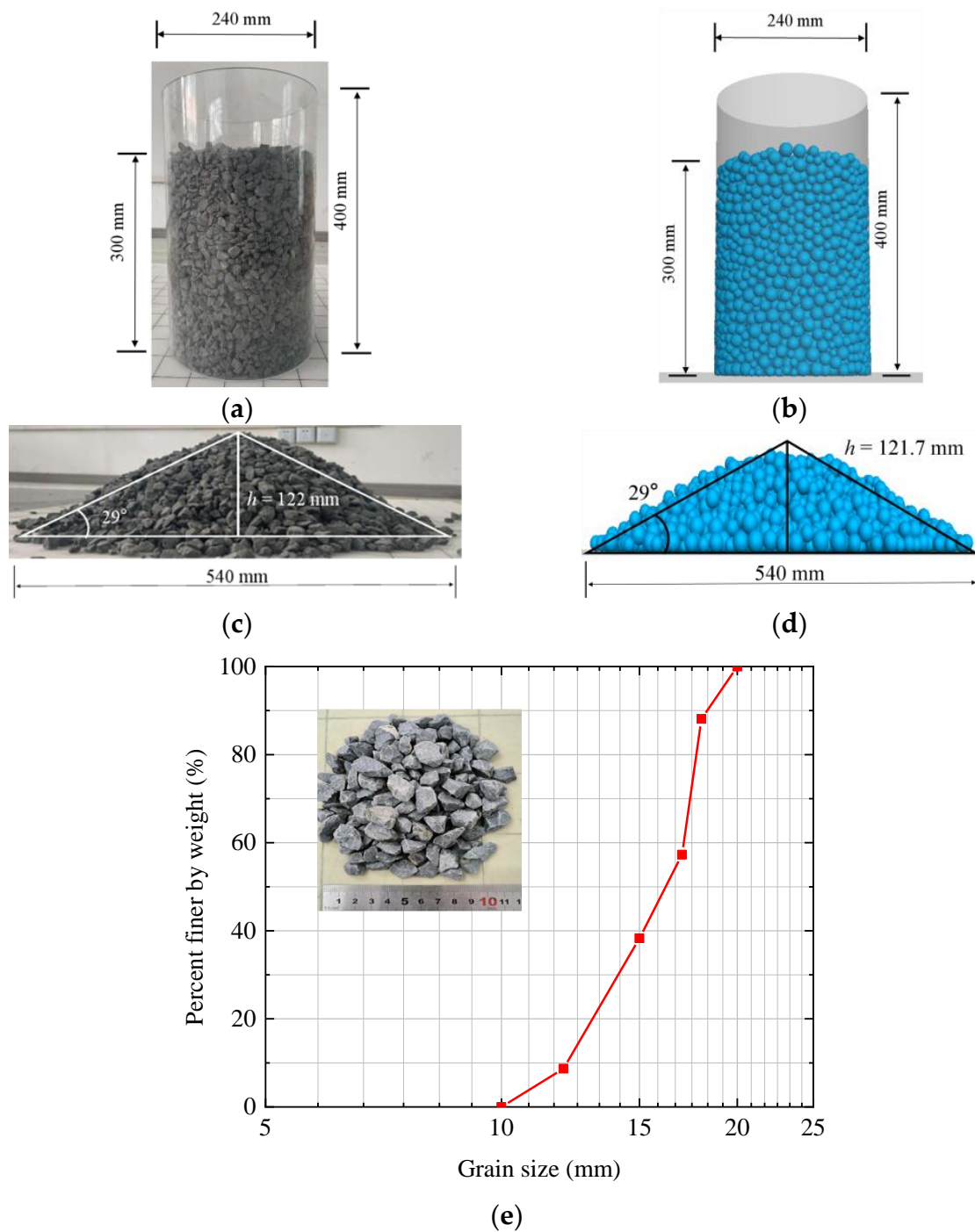


Figure 4. Comparison of test results and PFC numerical results of the granular column collapse. (a) Granular column collapse test; (b) PFC model of the granular column collapse test; (c) experimental heap morphology; (d) simulated heap morphology; (e) grading curve of the granular material.

3. Results

3.1. Influence of Slope Angle

The motion velocity, impact force, and other characteristics of debris flows are significantly influenced by the slope angle. To analyze the influence of slope angle, granular flow experiments are conducted at five angles: 40°, 45°, 50°, 55°, and 60°. To analyze the velocity evolution of the granular flows, a total of 20 particles at the front edge of the granular flow are monitored. The time history of the average velocity of monitored particles is shown in Figure 5.

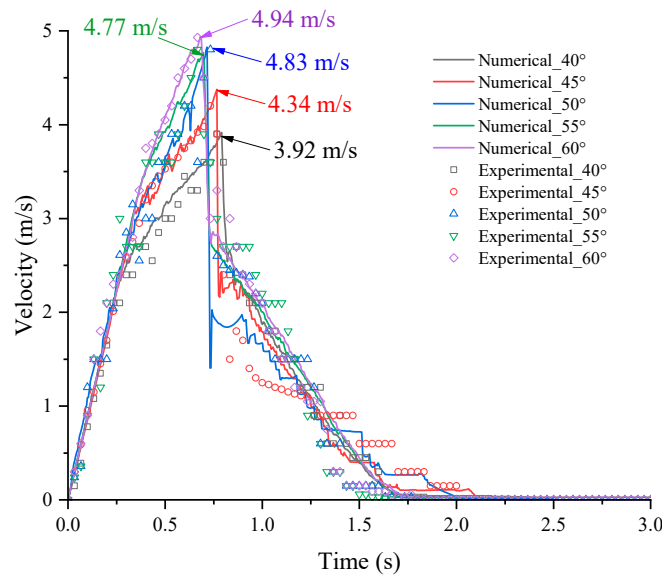


Figure 5. Velocity time history of the granular flow at different slope angles.

3.1.1. Movement Velocity

Figure 5 shows the velocity time history curves of the leading edge of granular flows naturally sliding without a shed tunnel for five different angles. From the figure, it can be observed that the numerical simulation results are in good agreement with the model test data. The time to reach the peak velocity is around 0.7 s, and it slightly advances with an increase in the slope angle. The peak velocity increases as the slope angle increases, reaching 3.92 m/s at 40° and 4.94 m/s at 60°. Once the front of the granular flow contacts the bottom plate of the flume, the velocity rapidly decreases and comes to a complete stop after moving a certain distance.

3.1.2. Impact Force

Figure 6 shows a comparison between the model test and numerical simulation results of the granular flow impacting a shed tunnel at a 45° angle. The high level of agreement throughout the entire process indicates that the parameters are reasonable and can accurately reflect the real sliding behavior of the granular materials. The entire impact process can be divided into the following stages: pre-impact; granular flow impacts the shed; a dead zone forms; continued rearward impact; the dead zone reaches the shed tunnel top; particle overflow; and deceleration and cessation. In the early stage of granular flow impacting the shed tunnel, the primary source of frontal normal impact force is the direct collision of particles. However, once a larger dead zone is formed, the frontal normal impact force is mainly generated by the rear portion of the granular flow impacting the dead zone and then indirectly transmitted to the tunnel.

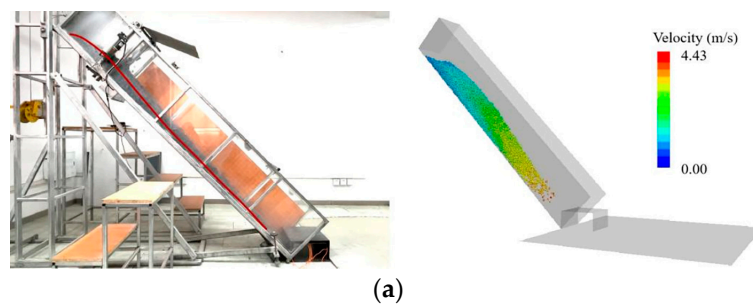


Figure 6. Cont.

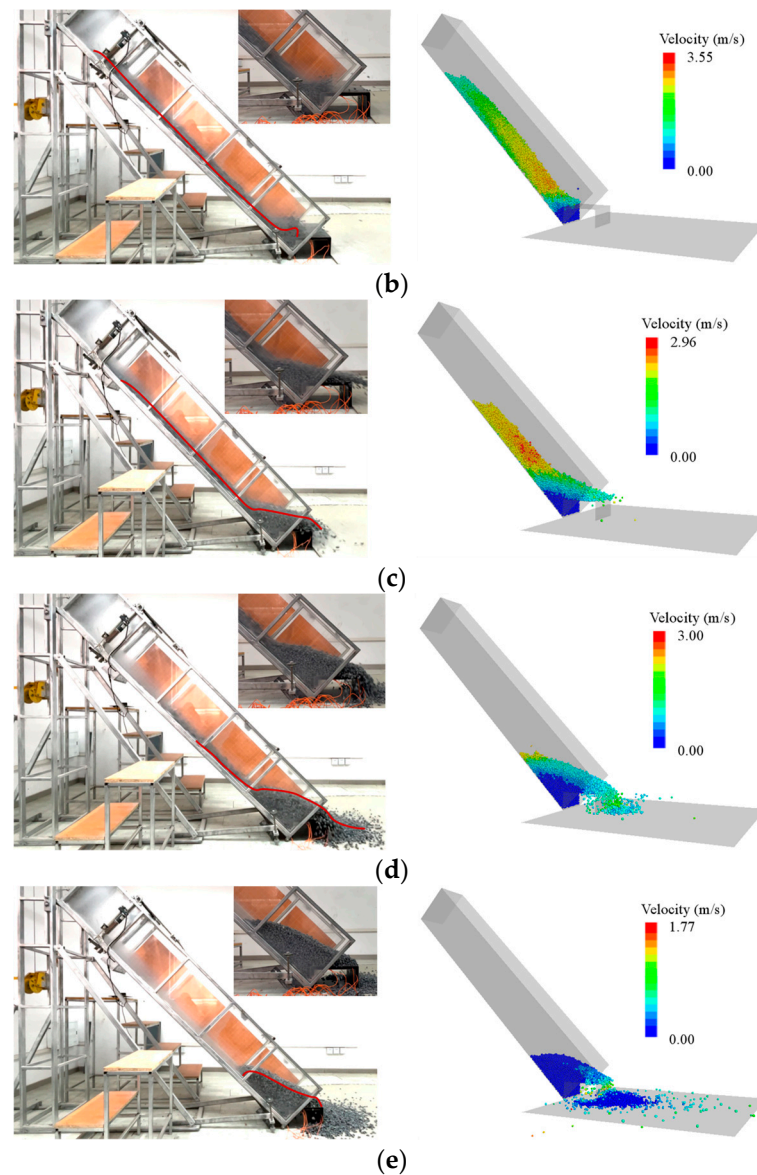


Figure 6. Snapshots of the granular flow in the experimental test and numerical simulation. (a) $t = 0.7$ s; (b) $t = 1.0$ s; (c) $t = 1.3$ s; (d) $t = 1.6$ s; (e) $t = 2.5$ s.

According to the velocity analysis and the relationship between velocity and impact force, it is evident that the impact force of the granular flow varies with different slope angles. Figure 7a shows the time history curves of the frontal normal impact force for each angle. It is apparent that both the peak impact force and residual force increase with the angle. For instance, at a slope angle of 60° , the peak impact force and residual force are approximately 565 N and 324 N, respectively, which are 3.3 times and 2.1 times higher than those at 40° . At smaller angles, the time history curves of the impact force do not exhibit distinct peaks. However, as the slope angle increases to 50° , a peak appears, and the higher the slope angle, the more pronounced the peak becomes. This is because at larger slope angles, the granular flow attains higher peak velocity and greater kinetic energy, resulting in more intense impacts on the shed tunnel.

The time history curve of the normal impact force on the top surface of the shed tunnel is shown in Figure 7b. The peak impact force increases with an increase in the slope angle, but the amplitude is not as significant as that of the frontal normal impact force. For example, at a slope angle of 60° , the peak impact force is around 225 N, which is 2.2 times higher than that at 40° . Furthermore, the time at which the impact force reaches its peak

varies significantly with different slope angles. As the slope angle increases, the moment of impact on the top surface of the shed tunnel occurs earlier, and the advance is slightly greater than that of the frontal normal impact. After 2.0 s, the impact force gradually stabilizes, and the differences in impact force among the five angles are not significant, with all values being around 100 N. This is because after the granular flow comes to a rest, the residual force of the normal impact force on the top surface mainly comes from the self-weight of the particles accumulated on the top surface, and the volume of granular flow particles deposited on the top surface does not differ significantly among the five cases.

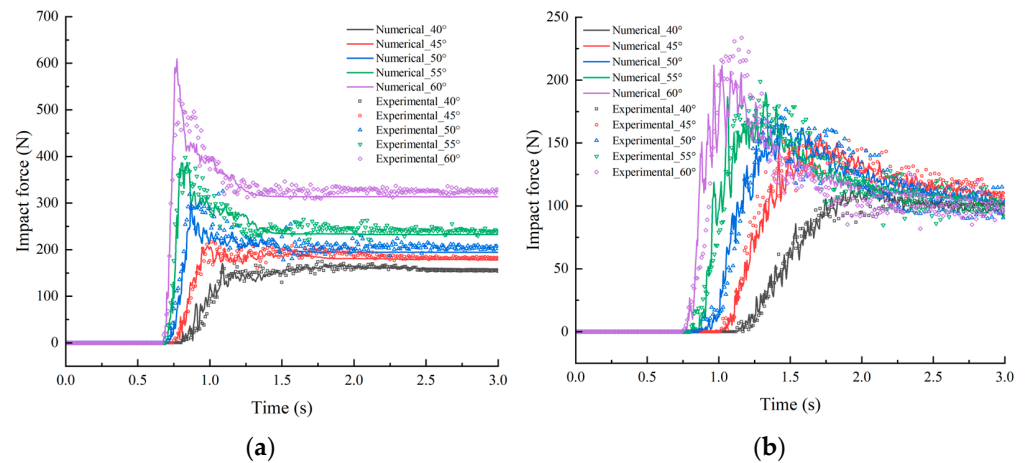


Figure 7. Impact force time history of the granular flow on the shed tunnel at different slope angles. (a) Normal impact force on the frontal surface; (b) normal impact force on the top surface.

3.2. Influence of the Cushion Layer

To mitigate the impact of granular flow on the shed tunnel, it is common in engineering to use locally available materials such as gravel soil or sandy soil to construct a cushion layer. This study aims to investigate the influence of cushion layer thickness and particle size on the granular flow impact force.

3.2.1. Thickness of the Cushion Layer

The thickness of the cushion layer directly affects its buffering effect. Therefore, in this study, the thickness of the cushion layer is roughly divided into two types. The first type is only laid between the flume and the shed tunnel, with a thickness not exceeding the height of the shed tunnel, as shown in Figure 8a–c. We selected three thicknesses: 50 mm, 100 mm, and 150 mm. The second type is laid between the flume and the shed tunnel and on the top surface of the shed tunnel. The thickness of this type is 200 mm, and the particle size of the cushioning layer is selected to be 10 mm to 20 mm, as shown in Figure 8d.

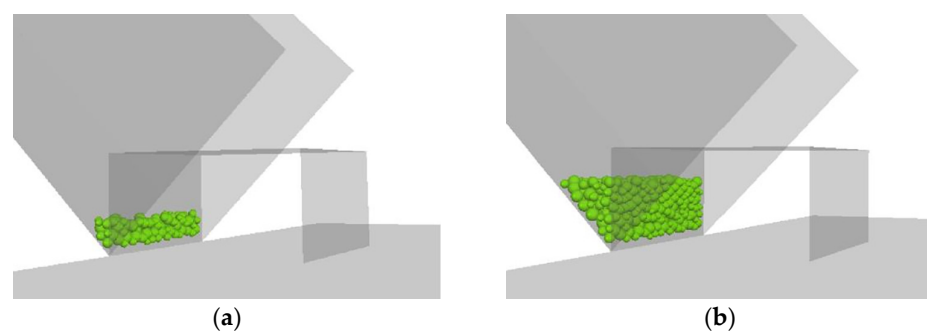


Figure 8. Cont.

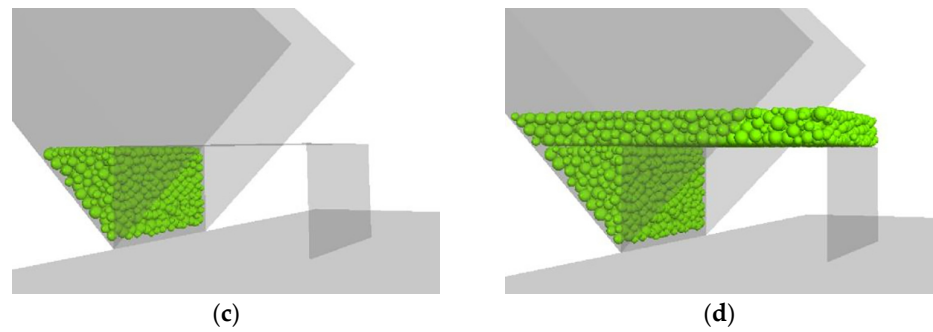


Figure 8. Schematic of cushion layers with different thicknesses. (a) 50 mm; (b) 100 mm; (c) 150 mm; (d) 200 mm.

Figure 9a shows the time history curves of the frontal normal impact force on the shed tunnel for different cushion layer thicknesses. Except for the cases without a cushion layer and with a 50 mm cushion layer, where the differences in impact force peak values are not significant, it is evident that the peak impact force as well as the residual value decrease with an increase in cushioning layer thickness. When the cushion layer thickness reaches 200 mm, the peak value and residual value of the frontal normal impact force on the shed tunnel are approximately 102 N and 89 N, respectively. Compared to the case without a cushion layer, the peak value and residual value decrease by approximately 50.7% and 50.0%, respectively. Therefore, it can be concluded that increasing the thickness of the cushion layer can effectively reduce the impact of the granular flow on the frontal section of the shed tunnel.

Figure 9b depicts the time history curves of the normal impact force on the shed tunnel top for different cushion layer thicknesses. When the cushion layer thickness is 0 mm, 50 mm, 100 mm, and 150 mm, there are no significant differences in the peak impact force, residual value, or their variations. However, when the cushion layer thickness reaches 200 mm, there is a noticeable decrease in the impact force. The peak value and residual value of the impact force are approximately 128 N and 64 N, respectively. Compared to the case without a cushion layer, the peak value and residual value of the impact force decrease by approximately 19.5% and 41.8%, respectively. This indicates that laying a cushion layer only between the shed tunnel and the flume has little effect on reducing the impact force on the top surface. It is only when the cushion layer covers the top surface of the shed tunnel that it can effectively provide buffering. Therefore, in practical engineering, it is necessary to increase the cushion layer thickness appropriately and lay cushion layers on both the frontal and top surfaces of the shed tunnel to better protect the shed tunnel from granular flow impact.

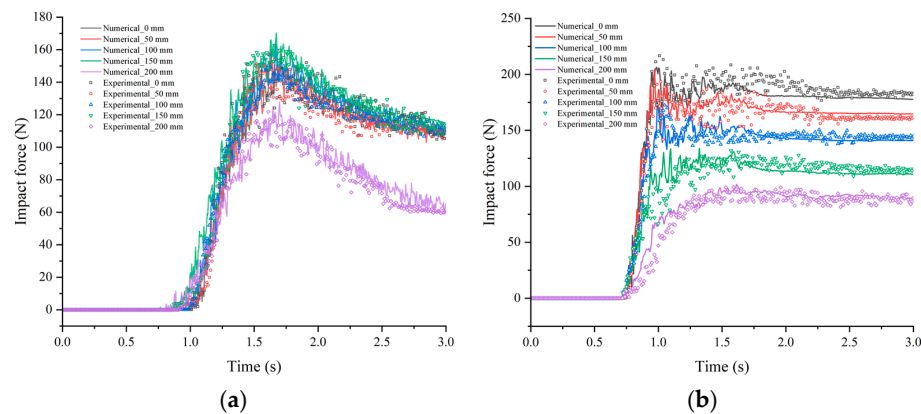


Figure 9. Impact force time history of the granular flow on the shed tunnel at different thicknesses of cushion layers. (a) Normal impact force on the frontal surface; (b) normal impact force on the top surface.

3.2.2. Particle Size of the Cushion Layer

To gain a deeper understanding of the buffering effect of cushion layers with different particle sizes, gravels with three different particle sizes, 3 mm~5 mm, 5 mm~10 mm, and 10 mm~20 mm, are used as cushion layer materials in this study. The cushion layer thickness is set at 200 mm.

Figure 10a shows the time history curves of the frontal normal impact force on the shed tunnel as the particle size of the cushion layer varies. None of the curves exhibit significant peaks. It can be observed that before 1.0 s, there was no significant difference in the impact force among the three cases. However, after that, there is a trend where the impact force decreases as the particle size of the cushion layer becomes smaller. The peak and residual values of the impact force for the fine particles are approximately 79 N and 73 N, respectively. Compared to the coarse particles, they are reduced by approximately 22.5% and 18.0%, respectively. This indicates that reducing the particle size of the cushion layer can further decrease the impact force. Comparing these results with the case without a cushion layer mentioned in Section 3.2.1, using a 200 mm cushion layer with fine particles reduces the impact force by more than half. The buffering effect is significant and can effectively protect the safety of the shed tunnel.

Figure 10b illustrates the time history curves of the impact force on the shed tunnel top as the particle size of the cushion layer varies. Compared to the frontal impact force, the differences in the impact force are relatively small. The peak values of the impact force decrease as the particle size of the cushion layer decreases, with values of 128 N, 109 N, and 101 N. The differences in the residual values of the impact force are minimal, but the trend is opposite to that of the peak values. As the particle size of the cushion layer decreases, there is a slow increase in the residual values.

The research has practical implications for the design and protection measures of shed tunnel structures. According to the results of this section, finer particles can provide a better cushioning effect and protect the shed tunnel structures from the impact of granular flow disasters.

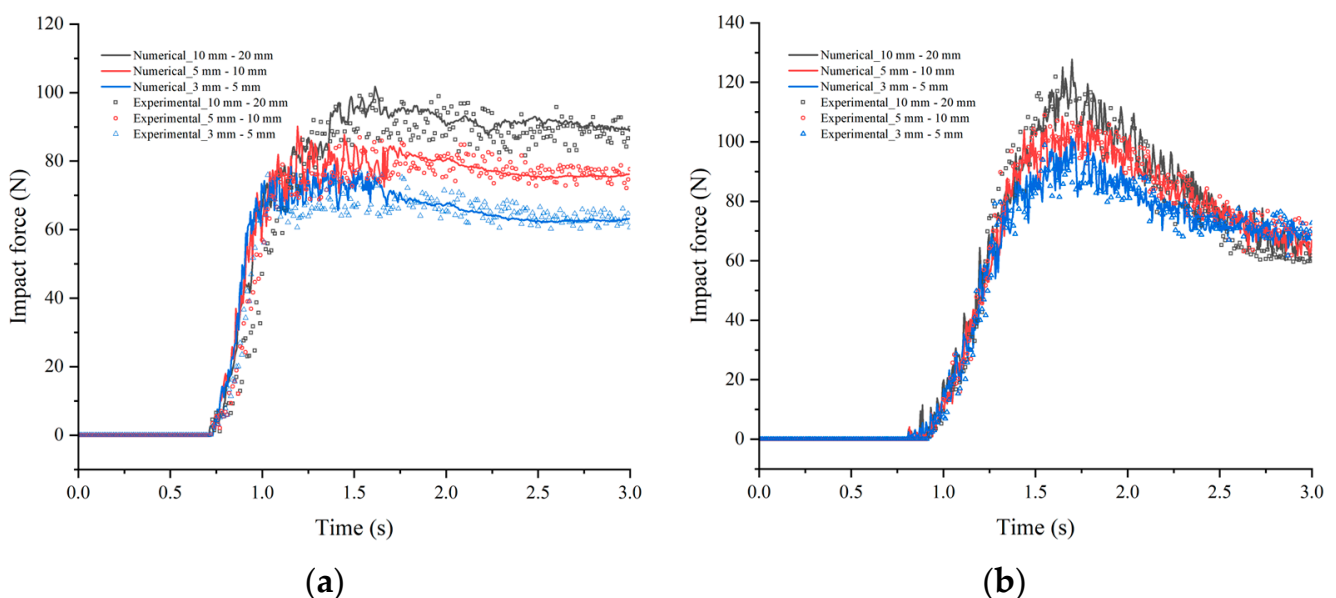


Figure 10. Impact force time history of the granular flow on the shed tunnel at different particle sizes of cushion layers. (a) Normal impact force on the frontal surface; (b) normal impact force on the top surface.

4. Discussion

4.1. Effectiveness of Cushioning

In this section, the buffering effects are analyzed based on the morphology of the granular flow and the cushion layer. Figure 11 presents the impact states, which are observed under different cushion layer thicknesses and particle sizes at six time points: 0.75 s, 0.80 s, 0.85 s, 0.90 s, 1.00 s, and 1.30 s.

When the cushion layer is composed of coarse particles with a thickness of 50 mm (Figure 11a), the interaction between the granular flow and the cushion layer is not significant due to the small thickness of the cushion layer. As a result, the granular flow quickly impacts the shed tunnel. This corresponds to the results of the frontal normal impact force peak values without a cushion layer and with a 50 mm cushion layer, as discussed in Section 3.2.1.

When the cushion layer consists of coarse particles with a thickness of 100 mm (Figure 11b), significant changes can be observed in the surface morphology of the cushion layer as the granular flow impacts it. Depressions appear near the flume, resulting in an overall convex shape. During this deformation process of the cushion layer, some of the energy of the granular flow is dissipated due to the friction between particles. However, since the thickness of the cushion layer is smaller than the height of the shed tunnel, the granular flow can still directly impact the shed tunnel after hitting the cushion layer. This can explain why, in Section 3.2.1, there is still a peak in the frontal normal impact force when using a 100 mm cushion layer.

As the thickness of the cushion layer reaches 150 mm, aligning its top surface with the shed tunnel top, as shown in Figure 11c, the deformation of the cushion layer after being impacted by the granular flow is similar to that of a 100 mm cushion layer. It eventually takes on a convex fan-shaped form. Since the thickness of the cushion layer is equal to the height of the shed tunnel, the granular flow cannot directly impact the frontal portion of the tunnel after hitting the cushion layer. Instead, it directly impacts the top of the shed tunnel along the cushion layer. In this case, the time history curve of the frontal normal impact force is relatively smooth, without any significant peaks.

When the thickness of the cushion layer is 200 mm, as shown in Figure 11d,e, the cushion layer undergoes greater deformation and more particles are splashed upon impact. The granular flow is unable to directly impact the shed tunnel. In both cases, the time history curves of the normal impact force are smaller compared to the previous three cases. In the case of a fine particle cushion layer, the smaller particle size results in a larger surface area, allowing for more friction between the particles, which leads to a better buffering effect. The final surface morphology of the cushion layer is more irregular compared to the case with coarse particles.

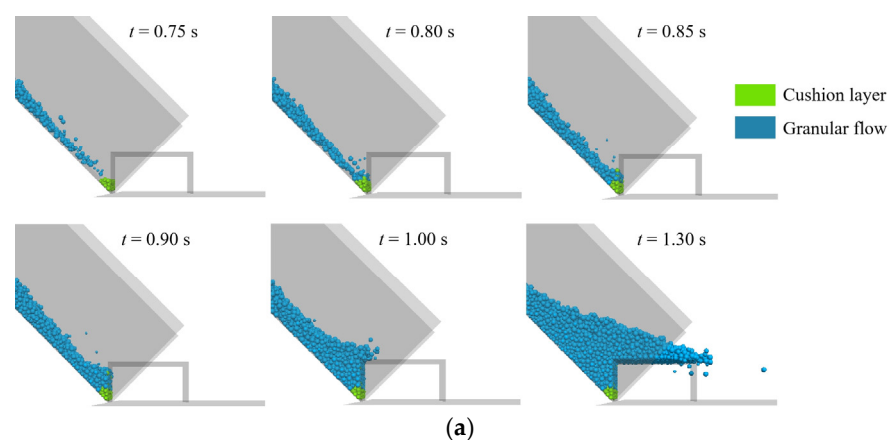


Figure 11. Cont.

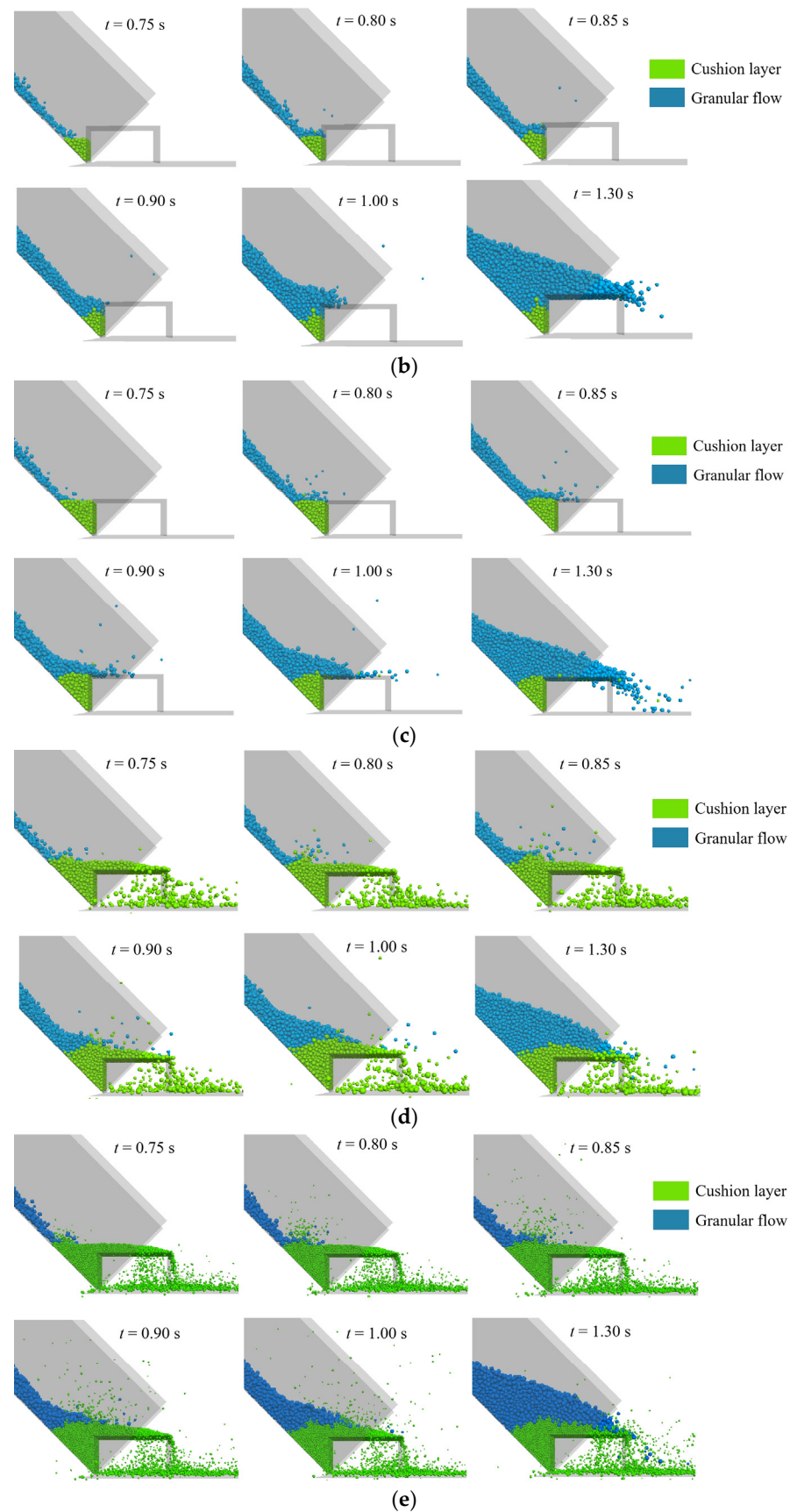


Figure 11. Variations in the morphology of cushion layers with different thicknesses and particle sizes during the impact process. (a) 50 mm coarse cushion layer; (b) 100 mm coarse cushion layer; (c) 150 mm coarse cushion layer; (d) 200 mm coarse cushion layer; (e) 200 mm fine cushion layer.

4.2. Energy Characteristics

In this study, the energy transfer mechanism throughout the entire process of granular flow motion is evaluated using the built-in energy tracking program in PFC3D. According to the principle of energy conservation, gravitational potential energy is converted into frictional energy, collision energy, kinetic energy, and other forms of energy consumption during the motion of granular flows. The analysis focused on dynamic impact and buffering effects from an energy perspective.

During a dynamic analysis, the kinetic energy at every time step is calculated as follows:

$$E_k = \frac{1}{2} m_k v_k^2 \tag{1}$$

where E_k is the kinetic energy, m_k is the elemental mass of particles, and v_k is the velocity at the midpoint of the element.

The total energy dissipated by collisions between particles is represented by the dashpot energy, calculated as follows:

$$E_p = \frac{1}{2} m_k^p (\eta_n v_k^{pn})^2 + \frac{1}{2} m_k^p (\eta_t v_k^{pt})^2 \tag{2}$$

where E_p is the dashpot energy; m_k is the elemental mass of particles; η_n and η_t , respectively, represent the normal and tangential damping ratios; and v_k^{pn} and v_k^{pt} are the velocity components of particle k along the normal and tangential directions, respectively.

Figure 12 shows the time history curves of the kinetic energy and dashpot energy of the granular flow at different slope angles without a cushion layer. From the graph, it can be observed that as the slope angle increases, the kinetic energy of the granular flow rapidly increases. The peak kinetic energy at a slope angle of 60° is 3.74 times higher than that at 40°. Additionally, with increasing the slope angle, the time to reach the peak kinetic energy gradually advances. In the time history curve of the dashpot energy, there is a distinct differentiating point. Before this point, there was not much difference in the dashpot energy of the granular flow at different angles. However, after this point, a phenomenon occurs where the dashpot energy increases with increasing the slope angle. The dashpot energy reflects the intensity of collisions between particles and between particles and the walls in the linear parallel bond model. Therefore, it can be inferred that as the slope angle increases and the granular flow impacts the shed tunnel, the collisions between particles and between particles and the shed tunnel become more intense, resulting in higher dashpot energy. This conclusion aligns well with the trend of the impact force on the shed tunnel varying with the slope angle.

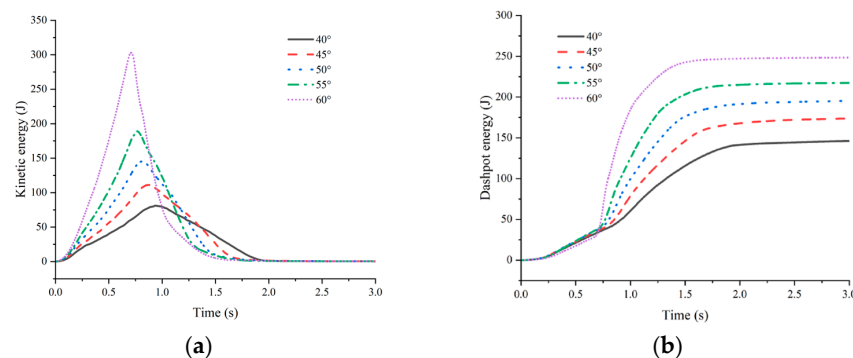


Figure 12. Kinetic energy and dashpot energy time history at different slope angles. (a) Kinetic energy; (b) dashpot energy.

Figure 13a depicts the time history curves of the kinetic energy for different cushion layer thicknesses. Before reaching the peak, the upward trend of the kinetic energy is mostly consistent across the five scenarios. After the peak, the downward trend shows

little variation among the different cases. The peak value of the kinetic energy decreases with the increasing cushion layer thickness, indicating that the cushion layer can reduce the overall kinetic energy of the debris flow to some extent through particle collisions and friction. Ultimately, this helps to decrease the impact force. From Figure 13b, it can be observed that the dashpot energy shows little difference among the four cases with cushion layer thicknesses of 0 mm, 50 mm, 100 mm, and 150 mm. However, when the cushion layer thickness reaches 200 mm and covers the top of the shed tunnel, the latter half of the dashpot energy curve differs from the other four cases. This is because when the cushion layer does not cover the top of the shed tunnel, although the impact on the frontal portion of the shed tunnel decreases, the top of the shed tunnel still experiences direct impact. As a result, the dashpot energy shows little variation. In contrast, when the cushion layer covers the top, the granular flow cannot directly impact the top of the structure. Therefore, the collisions between the granular flow and the shed tunnel are somewhat weakened, leading to a reduction in the dashpot energy.

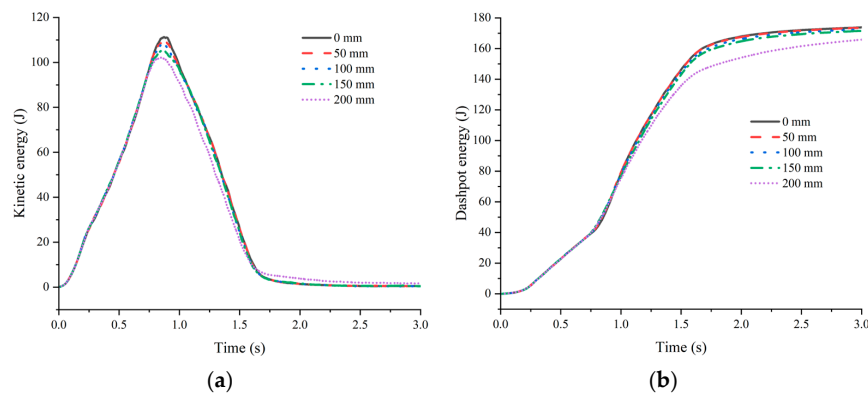


Figure 13. Kinetic energy and dashpot energy time history at different thicknesses of cushion layers. (a) Kinetic energy; (b) dashpot energy.

Figure 14 shows the time history curves of the kinetic energy and dashpot energy for different particle sizes of the cushion layer. It can be observed that the differences in kinetic energy among the three cases are not significant. Before reaching the peak, there is almost no difference in kinetic energy. In the descending phase, the kinetic energy decreases slightly faster with the smaller particle sizes of the cushion layer. Regarding the dashpot energy, there is no difference among the three cases until around 1.5 s. After that, there is a decreasing trend in dashpot energy as the particle size of the cushion layer decreases, which indicates a weakening of collisions between particles and between particles and the shed tunnel.

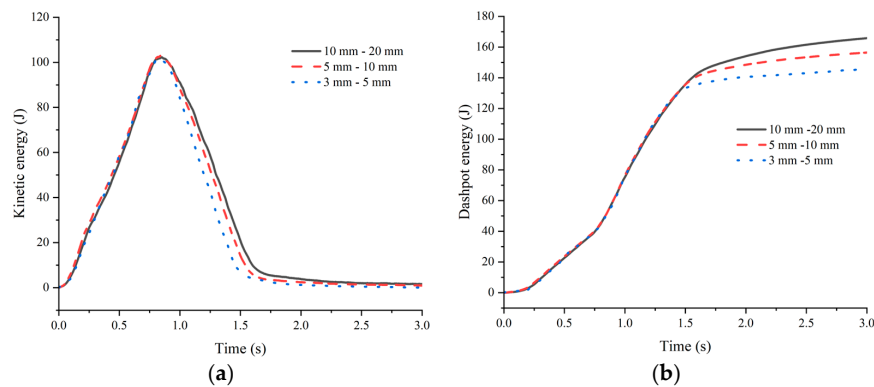


Figure 14. Kinetic energy and dashpot energy time history at different particle sizes of cushion layers. (a) Kinetic energy; (b) dashpot energy.

4.3. Limitations

This study investigates the impact force of granular flow on shed tunnels and the buffering effect of cushion layers using physical model experiments and PFC simulations. As an efficient method, physical model experiments are widely used to investigate the mechanisms of granular flow disasters. However, this method is often hindered by space limitations because it is difficult to build a large-scale model that accurately simulates natural processes. In PFC simulations, particles are assumed to be rigid, yet in the real world, rock masses are prone to breakage from interparticle collisions and impacts during propagation. Moreover, it is difficult to determine the micro-parameters of the PFC particles because they cannot be directly measured by laboratory tests. Therefore, although physical model experiments and PFC simulations provide an effective combined approach to investigating granular flow impact behavior on the shed tunnel, it is crucial to be aware of the limitations and assumptions. To ensure the reliability and applicability of the results, further validation and supplementation should be carried out by combining other methods, such as field experiments.

5. Conclusions

This study investigated the impact force of granular flow on a shed tunnel through model experiments and PFC simulations. The effects of slope angle, cushion layer thickness, and particle size on impact forces and the buffering effect of the cushion layer were discussed. The main findings of the study are as follows:

- (1) As the slope angle increases, both the peak velocity and the impact force of the granular flow on the shed tunnel increase significantly. Increasing the slope angle from 40° to 60° , the peak velocity rises from 3.92 m/s to 4.94 m/s, indicating an increment of about 25%. Concurrently, the impact force also amplifies by 2–3 times. Additionally, an increase in slope angle leads to a rapid escalation in the kinetic energy of the granular flow. The peak kinetic energy at 60° is 2.74 times greater than that at 40° . A larger slope angle results in higher dashpot energy, indicating more intense collisions between particles and the shed tunnel.
- (2) The thickness of the cushion layer directly affects the buffering effect. The augmentation of the cushion layer thickness enhances resistance and damping, resulting in a significant reduction in the kinetic energy of the granular flow and reducing the interaction between the granular flow and the shed tunnel. This helps to reduce the impact of granular flow on the front face of the shed tunnel, thus protecting its structural integrity. When the cushion layer thickness reaches 200 mm, the peak and residual values of the impact force are reduced by 50.7% and 50.0%, respectively, compared to the case without a cushion layer. When the cushion layer covers the top of the shed tunnel, the buffering effect of the cushion layer will be better.
- (3) A smaller particle size of the cushion layer effectively reduces the impact force of the granular flow on the shed tunnel structure. For a cushion layer with particle sizes ranging from 3 mm to 5 mm, the peak and residual values of the impact force on the front wall of the shed tunnel are reduced by 22.5% and 18.0%, respectively, compared to the case with particle sizes ranging from 10 mm to 20 mm. The smaller particle size of the cushion layer generates more friction with the granular flow, resulting in a significant change in its surface morphology, which can effectively reduce kinetic energy and provide stronger buffering effects in the later stage of movement.

Author Contributions: Conceptualization, Z.D.; methodology, L.W. and J.W.; software, J.W.; validation, L.W.; investigation, L.W. and J.W.; data curation, L.W. and J.W.; writing—original draft preparation, L.W. and J.W.; writing—review and editing, L.W. and Z.D.; supervision, Z.D.; funding acquisition, Z.D. All authors have read and agreed to the published version of the manuscript.

Funding: This research was funded by the National Natural Science Foundation of China (grant number 42102318), the Shanghai Science and Technology Innovation Action Plan (21DZ1204202) and the

Program for Professor of Special Appointment (Eastern Scholar) at Shanghai Institutions of Higher Learning (grant number TP2019037).

Institutional Review Board Statement: Not applicable.

Informed Consent Statement: Not applicable.

Data Availability Statement: The raw data supporting the conclusions of this article will be made available by the authors on request.

Conflicts of Interest: The authors declare no conflicts of interest.

References

1. Hungr, O.; Leroueil, S.; Picarelli, L. The varnes classification of landslide types, an update. *Landslides* **2014**, *11*, 167–194. [[CrossRef](#)]
2. Zhang, Y.; Guo, C.; Lan, H.; Yao, X. Reactivation mechanism of ancient giant landslides in the tectonically active zone: A case study in southwest China. *Environ. Earth Sci.* **2015**, *74*, 1719–1729. [[CrossRef](#)]
3. Li, P.U.; Wang, J.; Hu, K.; Shen, F. Effects of bed longitudinal inflexion and sediment porosity on basal entrainment mechanism: Insights from laboratory debris flows. *Landslides* **2021**, *18*, 3041–3062. [[CrossRef](#)]
4. Ijaz, N.; Ye, W.M.; Rehman, Z.U.; Dai, F.C.; Ijaz, Z. Numerical study on stability of lignosulphonate-based stabilized surficial layer of unsaturated expansive soil slope considering hydro-mechanical effect. *Transp. Geotech.* **2022**, *32*, 100697. [[CrossRef](#)]
5. Mahmood, K.; Rehman, Z.U.; Farooq, K.; Memon, S.A. One dimensional equivalent linear ground response analysis—A case study of collapsed Margalla Tower in Islamabad during 2005 Muzaffarabad Earthquake. *J. Appl. Geophys.* **2016**, *130*, 110–117. [[CrossRef](#)]
6. Cruden, D.M.; Hungr, O. The debris of the Frank Slide and theories of rockslide-avalanche mobility. *Can. J. Earth Sci.* **1986**, *23*, 425–432. [[CrossRef](#)]
7. Brideau, M.A.; Pedrazzini, A.; Stead, D.; Froese, C.; Jaboyedoff, M.; van Zeyl, D. Three-dimensional slope stability analysis of south peak, Crownsnest pass, Alberta, Canada. *Landslides* **2011**, *8*, 139–158. [[CrossRef](#)]
8. Wang, F.W.; Sassa, K. Landslide simulation by a geotechnical model combined with a model for apparent friction change. *Phys. Chem. Earth Parts A/B/C* **2010**, *35*, 149–161. [[CrossRef](#)]
9. Boon, C.W.; Housby, G.T.; Uthi, S. New insights into the 1963 Vajont slide using 2D and 3D distinct-element method analyses. *Géotechnique* **2010**, *64*, 800–816. [[CrossRef](#)]
10. Wolter, A.; Stead, D.; Clague, J.J. A morphologic characterization of the 1963 Vajont Slide, Italy, using long-range terrestrial photogrammetry. *Geomorphology* **2014**, *206*, 147–164. [[CrossRef](#)]
11. Kojan, E. Mayunmarca rockslide and debris flow, Peru. *Rockslides Avalanches* **1978**, *14*, 315–361. [[CrossRef](#)]
12. Delaney, K.B.; Evans, S.G. The 2000 Yigong landslide (Tibetan Plateau), rockslide-dammed lake and outburst flood: Review, remote sensing analysis, and process modelling. *Geomorphology* **2015**, *246*, 377–393. [[CrossRef](#)]
13. Zhou, J.W.; Cui, P.; Hao, M.H. Comprehensive analyses of the initiation and entrainment processes of the 2000 Yigong catastrophic landslide in Tibet, China. *Landslides* **2016**, *13*, 39–54. [[CrossRef](#)]
14. Xu, Q.; Shang, Y.; van Asch, T.; Wang, S.; Zhang, Z.; Dong, X. Observations from the large, rapid Yigong rock slide-debris avalanche, southeast Tibet. *Can. Geotech. J.* **2012**, *49*, 589–606. [[CrossRef](#)]
15. Yin, Y.P. Researches on the geo-hazards triggered by Wenchuan earthquake, Sichuan. *J. Eng. Geol.* **2008**, *16*, 433–444.
16. Xu, C.; Dai, F.C.; Xu, X.W. Wenchuan earthquake-induced landslides: An overview. *Geol. Rev.* **2010**, *56*, 860–874.
17. Fan, X.M.; van Westen, C.J.; Xu, Q.; Tolga, G.; Dai, F.C. Analysis of landslide dams induced by the 2008 Wenchuan earthquake. *J. Asian Earth Sci.* **2012**, *57*, 25–37. [[CrossRef](#)]
18. Mather, A.E.; Hartley, A.J.; Griffiths, J.S. The giant coastal landslides of Northern Chile: Tectonic and climate interactions on a classic convergent plate margin. *Earth Planet. Sci. Lett.* **2014**, *388*, 249–256. [[CrossRef](#)]
19. Naito, N.; Maeda, K.; Konno, H.; Ushiwatari, Y.; Suzuki, K.; Kawase, R. Rockfall impacts on sand cushions with different soil mechanical characteristics using discrete element method. *Soils Found.* **2020**, *60*, 384–397. [[CrossRef](#)]
20. Bhatti, A.Q. Falling-weight impact response for prototype RC type rock-shed with sand cushion. *Mater. Struct.* **2015**, *48*, 3367–3375. [[CrossRef](#)]
21. He, S.M.; Shen, J.; Wu, Y. Rock shed dynamic response to impact of rock-fall. *Rock Soil Mech.* **2011**, *32*, 781–788.
22. Gottardi, G.; Govoni, L. Full-scale modelling of falling rock protection barriers. *Rock Mech. Rock Eng.* **2010**, *43*, 261–274. [[CrossRef](#)]
23. Chen, T.J.; Xiang, X.; Zhang, G.C. Hertz theory based study on punching characteristics of rockfall impacting on shed-tunnel structure. *J. Eng. Geol.* **2023**, *31*, 199–206.
24. Wang, L.F.; Liu, L.; Tang, F.; Tang, H.M. Study on impact force of rockfall impact experiment on shed tunnel. *J. Disaster Prev. Mitig. Eng.* **2018**, *38*, 973–979.
25. Wang, H.; Guo, C.; Wang, F.; Ni, P.; Sun, W. Peridynamics simulation of structural damage characteristics in rock sheds under rockfall impact. *Comput. Geotech.* **2022**, *143*, 104625. [[CrossRef](#)]
26. Song, Y.; Jiang, Y.J.; Wang, M. Buffering effect of gravel cushion layer on the impact of dry granular flow against a rock shed. *Chin. J. Rock Mech. Eng.* **2018**, *37*, 2359–2369.

27. Jiang, Y.J.; Song, Y.; Ning, P.; Wang, Z.Z. Research on the buffering measure of rock shed against the impact of dry granular flow with concern of structure damage. *Landslides* **2022**, *19*, 2605–2627. [[CrossRef](#)]
28. Liu, C.; Yu, Z.; Zhao, S. Consideration of maximum impact force design for a rock shed against dry granular flow. *Eur. J. Environ. Civ. Eng.* **2022**, *26*, 2963–2984. [[CrossRef](#)]
29. Jiang, Y.J.; Wang, Z.Z.; Song, Y.; Xiao, S.Y. Cushion layer effect on the impact of a dry granular flow against a curved rock shed. *Rock Mech. Rock Eng.* **2018**, *51*, 2191–2205. [[CrossRef](#)]
30. Khasraghy, S.G.; Kishi, N.; Vogel, T. Numerical Simulation of Consecutive Rockfall Impacts on Reinforced Concrete Slabs. In *IABSE Symposium Bangkok 2009. Sustainable Infrastructure. Environment Friendly, Safe and Resource Efficient International Association for Bridge and Structural Engineering Chulalongkorn University, Thailand Asian Institute of Technology; National Academy of Sciences: Washington, DC, USA, 2009.*
31. Kishi, N.; Okada, S.Y.; Kon-No, H. Numerical impact response analysis of rockfall protection galleries. *Struct. Eng. Int.* **2009**, *19*, 313–320. [[CrossRef](#)]

Disclaimer/Publisher’s Note: The statements, opinions and data contained in all publications are solely those of the individual author(s) and contributor(s) and not of MDPI and/or the editor(s). MDPI and/or the editor(s) disclaim responsibility for any injury to people or property resulting from any ideas, methods, instructions or products referred to in the content.